Journal of Visualization, Vol. 8, No. 1 (2005)33-40

Numerical Simulation of Flow in a Screw-Type Blood Pump

Kilani, M. I.*[1], Haik, Y. S.*[2], Jaw, S-Y.*[3] and Chen, C-J.*[4]

*1 Mechanical Engineering Department, University of Jordan, Amman 11942 Jordan.
E-mail: mkilani@ju.edu.jo
*2 Center for Nanomagnetics and Biotechnology, Tallahassee 32310 Florida, USA.
E-mail: haik@eng.fsu.edu
*3 National Taiwan Ocean University, Keelung, Taiwan, R.O.C. E-mail: shjaw@eng.fsu.edu
*4 FAMU-FSU College of Engineering, Tallahassee 32310 Florida, USA. E-mail: cjchen@eng.fsu.edu

Received 2 August 2002
Revised 9 August 2004

Abstract : This study presents a numerical investigation of the flow field in a screw pump designed to circulate biological fluid such as blood. A simplified channel flow model is used to allow analysis using a Cartesian set of coordinates. Finite analytic (FA) numerical simulation of the flow field inside the channel was performed to study the influence of Reynolds number and pressure gradient on velocity distribution and shear stresses across the channel cross-section. Simulation results were used to predict flow rates, circulatory flow and the shear stresses, which are known to be related to the level of red blood cell damage (hemolysis) caused by the pump. The study shows that high shear levels are confined to small regions within the channel cross-section, but the circulatory nature of the flow causes an increased percentage of blood elements to pass through the high shear regions, and increases the likelihood of cell damage.

Keywords : Screw pumps, blood flow, blood hemolysis, finite analytic method, flow simulation.

1. Introduction

Several investigators have successfully demonstrated the application of screw pump mechanisms for blood transport during the past decade (e.g., Jarvik et al., 1998, and Wampler et al., 1988). Screw pumps are valve-less, seal-less, have only one moving part, and have no pockets where blood can accumulate. Owing to their compactness and simplicity, screw pumps have received serious attention in blood transport applications and several new designs are being explored (e.g. Debakey, 2000).

Figure 1 depicts a schematic diagram of a typical screw pump. The pump consists of a single screw that rotates inside a close fitting barrel. The rotation of the screw moves the fluid forward in the channel between the screw core and the barrel and increases its hydrostatic pressure. Fluid in a screw pump is contained within a system that has both a moving boundary (surfaces of the screw) and a stationary boundary (barrel surface); hence, a drag flow is established in the fluid due to its viscosity.

This study investigates the influence of screw speed and applied pressure head on pump flow rates and shear stress levels. Shear stress is related to the level of cell damage (hemolysis) of pumped blood (Loverett, 1972). The influence of positive and negative pressure heads on flow rate and shear stresses for a screw pump operating at different speeds is studied in detail. The intended application of the analyzed pump is in a blood cancer treatment device requiring a disposable pump capable of producing a maximum flow rate of 100 ml/min against a pressure head of 2kPa. The overall outer

dimensions of the pumping device are $20\times20\times100$ mm.

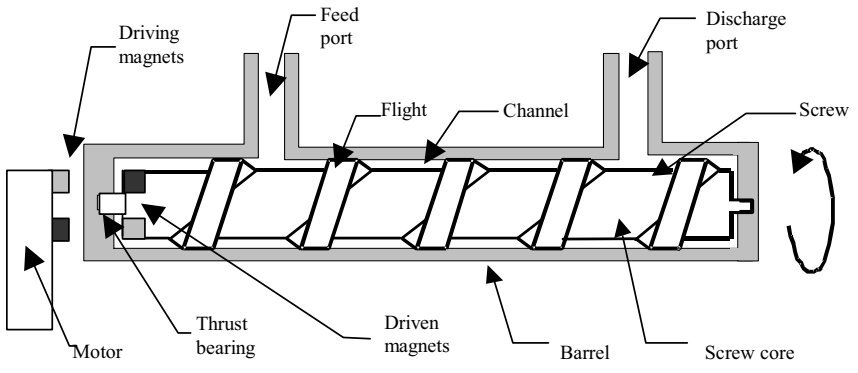

Fig. 1. Schematic diagram of a typical magnetically driven screw-type pump.

2. Screw Pump Geometry and Channel Flow Representation

Figure 2(a) shows part of the screw and the barrel and serves to define the screw geometry. D is the outer diameter of the screw, H is the screw channel depth, W and e are the channel width and the flight width, respectively, c is the radial clearance between the flight and the barrel, φ is the helix angle and L is the lead distance. An approximate simplifying representation is employed by which the screw channel is unrolled from the roots of the core and laid on a flat plate to form a rectangular channel as shown in Fig. 2(b). The flat plate located on top and in a parallel plane represents the barrel surface. The relative motion between the two planes causes the viscous effect needed for the pump to operate. The geometric assumptions made for this simplification are that H is small compared to D, which, in essence, causes the centrifugal force to be negligible compared to viscous forces, and allows the unrolled model described. The validity of this model for this case has been confirmed by several investigations (e.g. Fenner, 1977).

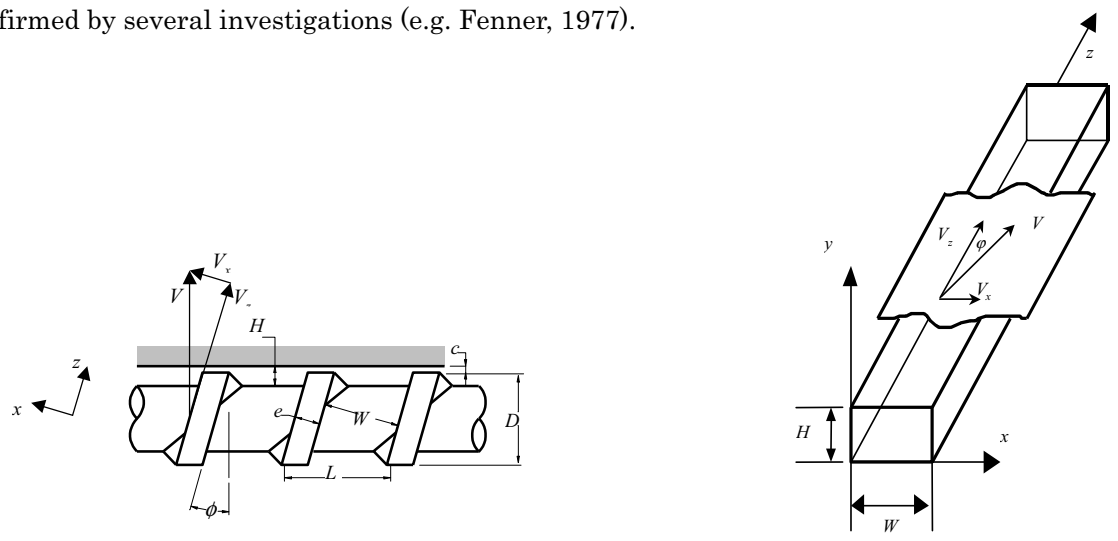

(a) (b)

Fig. 2. (a) Screw pump geometry and (b) Channel flow representation.

The study focuses on the contribution of the channel geometry on hemolysis, and ignores that occurring in the gap between the channel and the wall. While it is appreciated that the region between the blade tip and the wall represents a high shear region that cause appreciable cell damage for the blood passing through that gap, the percentage of blood flow through the gap is significantly smaller than the bulk of the flow, which occurs in the channel itself. Thus, the approximation assumes zero radial clearance c, and ignores the flow between the blade tip and the wall.

3. Governing Equations and Boundary Conditions

The flow in a helical screw channel rotating with a frequency N is now reduced to that of a flow in a stationary straight rectangular channel covered by an infinite plate (the barrel) which moves with a constant velocity $V = \pi DN/2$ at a constant angle (equal to φ) relative to the channel axis. Using this model, the governing equations of fluid motion can be written using a Cartesian set of coordinates.

For the purpose of blood pumping, we assume that the characteristic length of the screw, for example $W = 5\ mm$ is much larger than that of blood cell size ~20 microns, so that blood can be treated as a homogeneous Newtonian fluid, and the steady Navier-Stokes equations are:

$$\frac{\partial u_i}{\partial x_i} = 0 \tag{1}$$

$$u_j \frac{\partial u_i}{\partial x_j} = \nu \frac{\partial^2 u_i}{\partial x_j \partial x_j} - \frac{1}{\rho}\frac{\partial p}{\partial x_i} \tag{2}$$

where $\nu = \mu/\rho$ is the kinematic viscosity of the fluid. Noting that the z is much larger than both x and y, and that the boundary conditions are independent of z, the relative variations along z are negligible and a fully developed flow in the z direction may be assumed, and the Navier-Stokes equations in dimensionless form become:

$$\frac{\partial u^*}{\partial x^*} + \frac{\partial v^*}{\partial y^*} = 0 \tag{3}$$

$$u^* \frac{\partial u^*}{\partial x^*} + v^* \frac{\partial u^*}{\partial y^*} = -\frac{\partial p^*}{\partial x^*} + \frac{1}{Re}\left(\frac{\partial^2 u^*}{\partial x^{*2}} + \frac{\partial^2 u^*}{\partial y^{*2}}\right) \tag{4}$$

$$u^* \frac{\partial v^*}{\partial x^*} + v^* \frac{\partial v^*}{\partial y^*} = -\frac{\partial p^*}{\partial y^*} + \frac{1}{Re}\left(\frac{\partial^2 v^*}{\partial x^{*2}} + \frac{\partial^2 v^*}{\partial y^{*2}}\right) \tag{5}$$

$$u^* \frac{\partial w^*}{\partial x^*} + v^* \frac{\partial w^*}{\partial y^*} = -\frac{\partial p^*}{\partial z^*} + \frac{1}{Re}\left(\frac{\partial^2 w^*}{\partial x^{*2}} + \frac{\partial^2 w^*}{\partial y^{*2}}\right) \tag{6}$$

where u^*, v^* and w^* are the velocities normalized by the velocity of the top plate $V = \left(V_x^2 + V_z^2\right)^{1/2}$, where $V_x = V\sin\varphi$ and $V_z = V\cos\varphi$. The dimensionless variable p^* is the pressure normalized by ρV^2 with ρ standing for the fluid density. The coordinates x^*, y^* and z^* are normalized with respect to the channel height H, and the parameter Re is Reynolds number defined by $Re = VH/\nu$. The boundary conditions resulting from non-slip condition on the walls of the channel can be written as

$$u^* = v^* = w^* = 0 \ \text{ on } x^* = 0,\ x^* = a,\ y^* = 0 \tag{7}$$

$$u^* = \sin\varphi,\ v^* = 0,\ w^* = \cos\varphi \ \text{ on } \ y^* = 1 \tag{8}$$

The solution for the four unknowns u^*, v^*, w^* and p^* as a function of x^*, y^* and z^* in the above model depends on the four parameters a, φ, dp^*/dz^* and Re. The first two parameters describe the geometry of the screw pump while the last two describe the operating conditions. It is further observed that Eq. (3) through Eq. (5) are independent of z, and are equivalent to those obtained in modeling a lid driven cavity problem. Both u^* and v^* are equivalent to those obtained from solution of the lid driven cavity and will be independent of the pressure gradient dp^*/dz^*.

4. Finite Analytic Formulation and Case Studies

A numerical solution based on the finite analytic (FA) method was generated for the fully developed, incompressible Newtonian flow in the screw channel. The FA method (Chen et. al., 2000) is based on subdividing the solution domain into a number of simple uniform rectangular sub-regions. The boundary nodes of each sub-region are assumed to satisfy simple prescribed conditions and the governing partial differential equations are locally linearized to form a well-posed linear boundary value problem over the sub-region. The analytical solution for the resulting boundary value problem is used as an interpolating function that relates the interior nodal values of each sub-region algebraically to its neighboring nodal values. A system of algebraic equations results from the previous steps, the solution of this system represents the numerical solution of the problem.

For the problem described, the solution domain is considered to be the x^*y^* plane with $0 \le x^* \le a$ and $0 \le y^* \le a$. The channel cross section was discretized using a uniform 60×60 grid at which grid independence was established. The computation was made using with time marching with a time step of 0.07. The steady solution was achieved when the numerical solution became time independent and when the mass source error in the continuity equation became below 5×10^{-5}.

Numerical simulation was performed on a screw pump with square channel and a helix angle $\varphi = 30^o$. Positive, zero and negative pressure gradients were simulated. Normally, a screw pump operates with positive pressure gradient along the screw channel. Zero pressure gradient implies that no pressure head is imposed on the pump and the flow through the screw channel is totally due to the drag effect of the screw rotation. Negative pressure gradients occurs under special conditions such as when the screw pump is used to accelerate an otherwise naturally occurring flow or to assist in the operation of other pumps within the system. For blood flow ($\rho = 1054$ kg/m^3) at a plate speed $V = 1.0$ m/s, $dp^*/dz^* = 10$ corresponds to a channel-wise pressure difference of 10.54 kPa/m. For a screw segment with $L = 100$ mm and $\varphi = 30^o$, such a pressure gradient represents a pressure difference of 2.108 kPa between the inlet and exit terminals of the channel.

Simulations were performed for $Re = 100$, $Re = 1000$ and $Re = 2000$. Physically, $Re = 1000$ represents blood flow ($\nu = 3.5 \times 10^{-6}$ m^2/s) in a screw pump with a $D = 20$ mm and $H = 3.5$ mm rotating at a speed of 100 rad/s ($N = 955$ rpm) (Plate velocity V= 1.0 m/s).

5. Results and Discussion

5.1 Axial velocity distribution

The longitudinal velocity distribution is of particular interest as it directly determines the flow rate of the pump. Figure 3 shows the longitudinal velocity contours for the three cases considered. The x and y axes in the figure correspond to the x^* and y^* axes of the channel cross-section, while the z axis represents the non-dimensional longitudinal velocity w^*. The longitudinal velocity profile starts flat at the top of the channel ($y^* = 1$) and drops rapidly in the top region where $0.9 \le y^* \le 1$. For $y^* < 0.9$, the longitudinal velocity declines gradually until it reaches zero at $y^* = 0$ in the bottom of the channel. For $dp^*/dz^* = 0$, w is always positive indicating a downstream flow direction across the whole channel cross-section. It is interesting to observe the zero velocity contour lines in Fig. 3(d) through Fig. 3(f). These lines take the shape of closed curves, which includes two walls of the channel. Outside the curve, the velocity is positive indicating forward flow. Inside the curve, the velocity is negative indicating back flow situation, which takes place in the case of an adverse pressure gradient.

A positive pressure gradient causes more rapid drop in the longitudinal velocity as we go down the channel. This is accompanied by a proportional decrease in the flow rate out of the screw pump. Figurre 4 depicts the calculated flow rates for the cases considered, and shows it to drop linearly with pressure gradient, while increasing with Re.

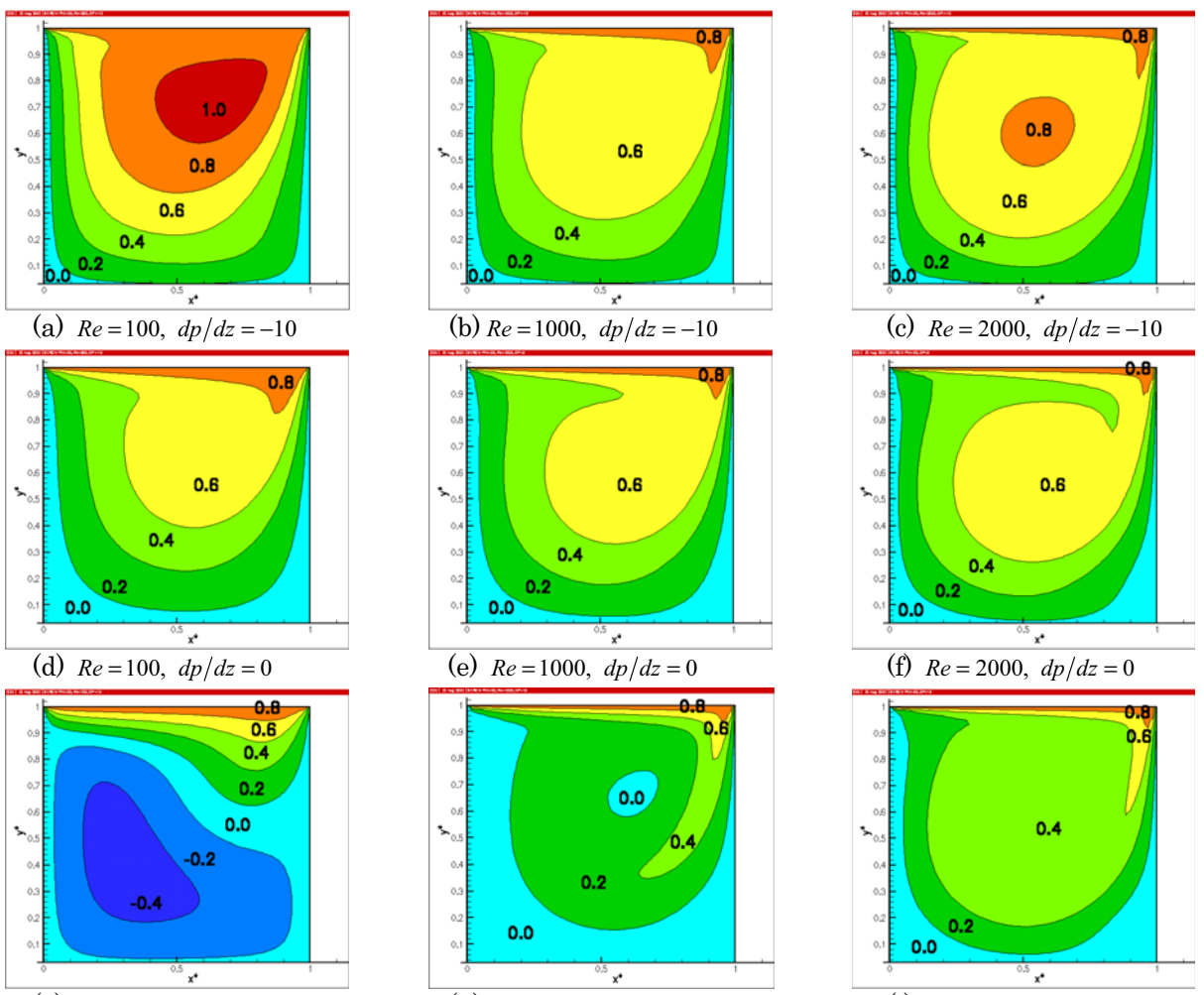

(a) $Re = 100,\ dp/dz = -10$ (b) $Re = 1000,\ dp/dz = -10$ (c) $Re = 2000,\ dp/dz = -10$

(d) $Re = 100,\ dp/dz = 0$ (e) $Re = 1000,\ dp/dz = 0$ (f) $Re = 2000,\ dp/dz = 0$

(g) $Re = 100,\ dp/dz = +10$ (h) $Re = 1000,\ dp/dz = +10$ (i) $Re = 2000,\ dp/dz = +10$

Fig. 3. Longitudinal velocity contours.

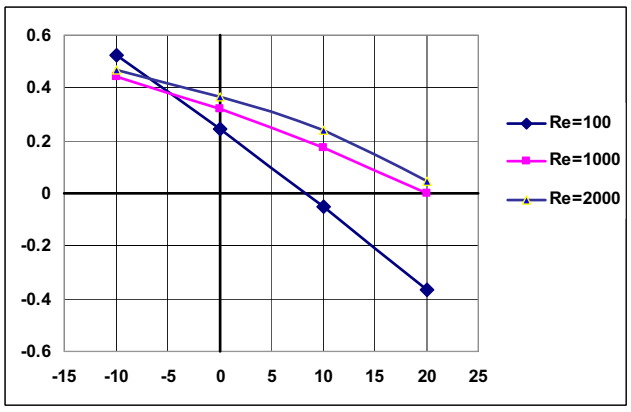

Fig. 4. Flow rate vs. pressure head.

5.2 Transverse velocity distribution

The transverse velocity components are superimposed on the longitudinal velocity component to cause a secondary circulatory flow within the screw channel. As shown in section 4, these

components are independent of dp^*/dz^* and resemble the field generated in a lid driven cavity flow with $Re_{cavity} = Re_x$. Figure 5 shows the transverse (u^*-v^*) velocity vectors for the values of Re examined. It is seen that the center of the circulatory flow shifts downwards with increased Re signifying an increased extent for circulatory flow. As Re increases, the effect of circulatory flow increases and tends to cover the whole cross section of the channel.

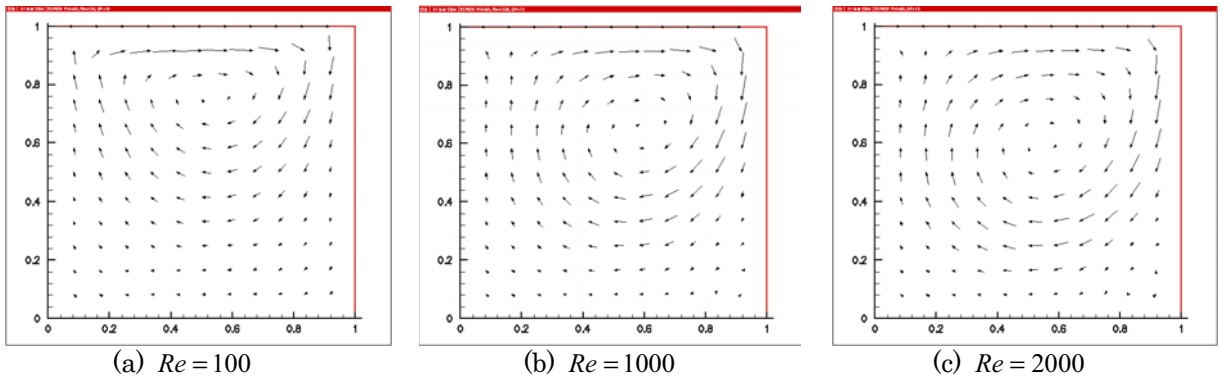

(a) $Re = 100$ (b) $Re = 1000$ (c) $Re = 2000$

Fig. 5. Transverse velocity field.

5.3 Shear stress distribution

The shear stress field across the channel can be calculated using its components:

$$\tau_{xy}^* = \frac{1}{Re}\left(\frac{\partial u^*}{\partial y^*} + \frac{\partial v^*}{\partial x^*}\right) \tag{9}$$

$$\tau_{xz}^* = \frac{1}{Re}\left(\frac{\partial w^*}{\partial x^*}\right) \tag{10}$$

$$\tau_{yz}^* = \frac{1}{Re}\left(\frac{\partial w^*}{\partial y^*}\right) \tag{11}$$

where τ_{ij}^* is the normalized stress tensor defined by: $\tau_{ij}^* = \tau_{ij}/\rho V^2$. Figure 6 depicts the shear stress components across the channel cross-section for the special case of $Re = 1000$ and $dp^*/dz^* = +10$. The figures show that the highest shear levels are localized in the regions near the walls of the channel. When considering blood flow, those figures should be interpreted in conjunction with the transverse velocity field figures of Fig. 5. For example, Fig. 5(b) depicts the transverse velocity of the flow for the case considered, and demonstrates the circulatory nature of the flow, which causes the blood elements to pass in and out of the high shear levels at a rate proportional to the speed of the pump.

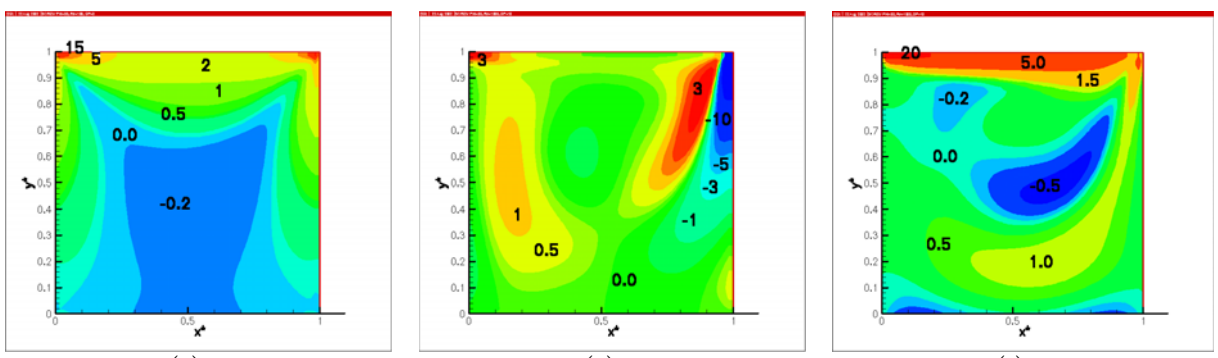

(a) τ_{xy}^* (b) τ_{xz}^* (c) τ_{yz}^*

Fig. 6. Shear components distribution *Re*=1000, *dp*/dz**=+10.

Figure 7 shows the variation of the magnitude of the shear stress tensor along the wall for the case considered. The horizontal axis in the figure ξ is a wall fitted coordinate that goes along the four sides of the channel. The figures demonstrate high local shear near the top left corner (point D) where τ^* approaches 60. It is important to compare this value with the threshold lytic shear stress for blood, τ_{lytic} defined as the maximum shear stress that a blood cell can withstand without rupture when exposed to for a period ($t<0.1$ *s*), and estimated to be around 2 kPa (Steinbach, 1970). Using the numerical values specified in section 4 for the top plate velocity $V=1$ m/s when $Re=1000$, and using a working fluid (blood) density $\rho=1054$ kg/m^3, a 2 kPa shear stress corresponds to a dimensionless shear stress of around 1.9×10^{-3}. It can be seen that this value is exceeded over significant regions within the channel. It is thus seen that τ_{lytic} is exceeded over a significant region near the top and side walls of the channel for $Re=1000$.

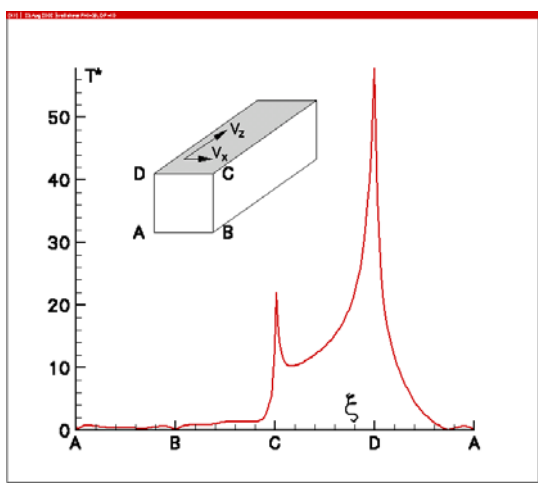

Fig. 7. Wall shear stress at *Re*=1000, *dp*/dz**=+10.

6. Conclusion

The paper presented a numerical simulation for fluid flow in a screw pump using the finite analytic method. A simplified channel flow model was used to allow the analysis of this problem using a Cartesian set of coordinates. Computational results produced predictions of the velocity field, shear stress distribution and circulatory flow.

The simulation revealed several important features of the flow in the screw channel. High magnitudes of shear stresses are developed in narrow bands in the channel closest to its boundaries while most of the interior region of the channel is under relatively lower shear stress. It may be argued that the existence of lower shear stress levels in the interior region of the channel could provide a safe transport mechanism for red blood cells in spite of exceeding the lytic threshold shear in the in the exterior regions. Such an argument would be based on the established fact that red blood cells tend to shift from high shear to low shear regions when present in a flow. In order for this to hold, however, the secondary circulatory flow in the channel demonstrated by Fig. 5 need to be minimized. Circulatory motion tends to carry red blood cells back into areas of high shear levels. The magnitude of the secondary flow is highly dependent on the helix angle of the screw. Lower helix angle leads to lower magnitudes of secondary flow velocities. Simulations results have shown that the secondary circulatory flow within the channel is not affected by changes in the pressure gradient. Secondary flow is determined by the transverse component of the velocity of the top plate. Future work includes a detailed study of the influence of screw geometry on pump performance. Accordingly, screw pump design can be optimized to satisfy flow rate and pressure requirement while simultaneously minimizing the rate of hemolysis produced by the pump.

References

Blackshear, P. L. and Blackshear G. L., Mechanical Hemolysis, Handbook of Bioengineering, by Skalak R. and Chien, S. editors, (1986).

Chen, C. J., Bernatz, B., Wanlai, L. and Kent, C., Finite Analytic Method in Flows and Heat Transfer, (2000), Taylor & Francis Inc, New York, New York.

Debakey, M. E., A miniature implantable axial flow ventricular assist device, The Annals of Thoracic Surgery, 68 (1999) 637-640.

Jarvik, R., Westaby, S, Katsumata, T, Pigott, D. and Evans R. D., LVAD Power Delivery: A Percutaneous Approach to Avoid Infection, The Annals of Thoracic Surgery, 65 (1998), 470-473.

Fenner, R. T., Developments in the analysis of steady screw extrusion of polymers, Polymer 18 (1977), 617-635.

Loverett, L. B., Hellums J. D., Alfrey, C. P. and Lynch, E. C., Red blood cell damage by shear stress Biophys J., 12 (1994), 257-273.

Kilani, M. I., Jaw, S. Y., Haik, Y. and Chen, C. J., Investigation of magnetically driven screw pumps for blood flow applications, 14th Engineering Mechanics Conference, ASCE, (Austin, Texas), (2000).

Steinbach, J., Hemolysis at tube walls, M. S. thesis, University of Minnesota, Minneapolis, St. Paul, (1970).

Wampler, D. G., Moise, J. C., Frazier, O. H. and Olesn, D. B., In vivo evaluation of a peripheral vasular access flow blood pump. ASAIO Trans 34 (1988), 450-454.

Author Profile

Mohammad Kilani: He received his M. Sc (Eng) in Mechanical Engineering in 1991 from Carnegie Mellon University in Pittsburgh, PA. He also received his Ph. D. in Mechanical Engineering from then Florida State University in Tallahassee, FL. He taught mechanical engineering in the University of Jordan, Amman, Jordan. He works on blood pump development and analysis, mechanical design, computer aided design, and micro-electro-mechanical systems (MEMS).

Yousef Haik: He is currently the Chair of the Department of Mechanical Engineering at the United Arab Emirates University. He is also a professor at the Florida State University. His research area includes application of nanomagnetics in biotechnology, MEMS and Biomagnetic Fluid Dynamics.

S-Y Jaw: He is a professor of the Systems and Naval Architecture Department of the National Taiwan Ocean University, Taiwan. He is active in such area as turbulence models, turbulence measurement technique, and color particle flow visualization.

C. J. Chen: He is the Dean of the FAMU-FSU College of Engineering. His research area includes turbulence modeling, heat transfer, CFD, Biomagnetic Fluids and micro systems.